Title

Anti-KIT DNA Aptamer for Targeted Labeling of Gastrointestinal Stromal Tumor

Journal

Molecular Cancer Therapeutics, 19(5)

ISSN

1535-7163

Authors

Banerjee, Sudeep

Yoon, Hyunho

Yebra, Mayra

et al.

Publication Date

2020-05-01

DOI

10.1158/1535-7163.mct-19-0959

Peer reviewed

HHS Public Access

Author manuscript

Mol Cancer Ther. Author manuscript; available in PMC 2020 November 01.

Published in final edited form as:

Mol Cancer Ther. 2020 May ; 19(5): 1173–1182. doi:10.1158/1535-7163.MCT-19-0959.

Anti-KIT DNA Aptamer for Targeted Labeling of Gastrointestinal Stromal Tumor

Sudeep Banerjee[1,2], **Hyunho Yoon**[1], **Mayra Yebra**[1], **Chih-Min Tang**[1], **Mara Gilardi**[3], **Jayanth S. Shankara Narayanan**[1], **Rebekah R. White**[1], **Jason K. Sicklick**[1,*,ℵ], **Partha Ray**[1,*,ℵ]

[1]Division of Surgical Oncology, Department of Surgery, Moores Cancer Center, University of California, San Diego, La Jolla, CA

[2]Department of Surgery, David Geffen School of Medicine at UCLA, Los Angeles, CA

[3]Moores Cancer Center, University of California San Diego, La Jolla, CA, USA

Abstract

Gastrointestinal stromal tumor (GIST), the most common sarcoma, is characterized by KIT protein overexpression, and tumors are frequently driven by oncogenic *KIT* mutations. Targeted inhibition of KIT revolutionized GIST therapy and ushered in the era of precision medicine for the treatment of solid malignancies. Here, we present the first use of a KIT-specific DNA aptamer for targeted labeling of GIST. We found that an anti-KIT DNA aptamer bound cells in a KIT-dependent manner and was highly specific for GIST cell labelling *in vitro*. Functionally, the KIT aptamer bound extracellular KIT in a manner similar to KIT monoclonal antibody staining, and was trafficked intracellularly *in vitro*. The KIT aptamer bound dissociated primary human GIST cells in a mutation agnostic manner such that tumors with *KIT* and *PDGFRA* mutations were labeled. Additionally, the KIT aptamer specifically labeled intact human GIST tissue *ex vivo*, as well as peritoneal xenografts in mice with high sensitivity. These results represent the first use of an aptamer-based method for targeted detection of GIST *in vitro* and *in vivo*.

Keywords

GIST; KIT; c-KIT; PDGFRA; oligonucleotide; targeted imaging; tumor imaging

Introduction

Gastrointestinal stromal tumor (GIST) is the most common sarcoma with ~3,000 new malignant cases in the United States annually (1). The treatment of GIST provided the first

ℵ**Co-corresponding authors:** Jason K. Sicklick, MD, FACS, Associate Professor of Surgery, Division of Surgical Oncology, Moores Cancer Center, University of California, San Diego, UC San Diego Health Sciences, 3855 Health Sciences Drive, Room 2313, Mail Code 0987, La Jolla, CA 92093-0987, Tel: 858-822-3967, Fax: 858-228-5153, jsicklick@ucsd.edu, Partha Ray, PhD, Assistant Adjunct Professor of Surgery, Moores Cancer Center, University of California, San Diego, UC San Diego Health Sciences, 3855 Health Sciences Drive, Room 2331, Mail Code 0803, La Jolla, CA 92093-0987, Tel: 917-907-4407, pray@ucsd.edu.

*Contributed equally.

Conflict of interest:

These disclosures had no impact on any of the work presented in this manuscript. There are no conflicts of interest to declare by the remaining authors.

proof of principle for precision medicine in solid tumors as oncogenic driver mutations in the *KIT* gene were identified and effectively targeted with a tyrosine kinase inhibitor (TKI), imatinib (IM). *KIT*-mutated GIST represents approximately 60–70% of disease and oncogenic KIT activation is associated with high levels of KIT expression (2,3). However, non-*KIT* mutant GIST also highly expresses KIT likely due to converging pathway activation (4). Currently, GIST diagnosis relies on analyzing tissue procured from either biopsy or surgical specimens. Although KIT-expressing GISTs are effectively diagnosed with immunohistochemical staining with anti-KIT antibodies, this approach requires ongoing hybridomas for production.

Aptamers are single-stranded oligonucleotide (DNA or RNA) ligands that are selected against specific targets (proteins, small molecules) through an *in vitro* iterative process called Systematic Evolution of Ligands by Exponential Enrichment (SELEX) (5,6). Aptamers undergo intra-molecular base-pairing between complementary nucleotides and assume secondary, followed by tertiary structures. In turn, these can bind to their cognate targets with high affinity and specificity similar to antibodies. In contrast, aptamers demonstrate enhanced tissue penetration due to their small sizes and are non-immunogenic as compared to antibodies. Aptamers are also amenable to a variety of chemical modifications and can be conjugated with compounds such as fluorophores or drugs. Thus, modified aptamers can be utilized for several applications including *in vitro* and *in vivo* imaging, as well as targeted drug delivery (7,8).

Recently, Zhao *et al.* presented a single-stranded DNA (ssDNA) aptamer that was developed for use in an acute myeloid leukemia (AML) model that highly expresses KIT (9). The investigators utilized a hybrid SELEX method that involves sequential exposure of a library of ssDNA oligonucleotides to AML cells *in vitro* followed by enrichment with recombinant KIT. In their study, the final selected oligonucleotide (aptamer) was conjugated to methotrexate and shown to be cytotoxic to AML lines and patient-derived samples. In another study, Tanno *et al.* used the same aptamer to develop a microRNA-aptamer chimera to deliver miR-26a against chemotherapy mediated myelosuppression (10). In both study studies, the anti-KIT aptamer was tested in the hematologic malignancies. However, the ability of an anti-KIT aptamer to bind and label solid tumor cells remains untested.

Here, we present a study of the utility of an anti-KIT aptamer in the detection of GIST. We find that the anti-KIT aptamer binds GIST cells in a KIT-dependent manner and is trafficked internally. Importantly, the aptamer binds to live and fixed primary human GIST cells, allowing for broad labelling applications. Lastly, we found that the KIT aptamer conjugated to a fluorophore can detect GIST cells both *ex vivo* and *in vivo*. This study provides the first proof of principle that an anti-KIT DNA aptamer may be used for targeted detection for human GIST, irrespective of driver mutation status.

Materials and Methods

Human Subjects

Written informed consent was obtained for all study participants, including publication of clinical data. Patient tissue collection, acquisition of clinical data, and conducting

experimental procedures on biological samples was approved by the UC San Diego Human Research Protections Program Institutional Review Board (IRB) (Protocol #181755). Pathological diagnosis was made by an experienced pathologist based on light microscopic analysis of Optimal Cutting Temperature (OCT) tissue sections and sections labeled with antibodies against KIT and DOG-1 (Discovered in GIST-1), a membrane associated antigen that is expressed in GIST irrespective of *KIT* or *PDGFRA* mutations (11). All experiments were conducted with de-identified tissues in accordance with appropriate regulatory guidelines for use of human tissue.

Aptamer Synthesis

Single stranded DNA KIT aptamer sequence was obtained from the primary literature report [5'-GAGGCATACCAGCTTATTCAAGGGGCCGGGGCAAGGGGGGGGTACCGTGGTAGGACATAGTAAGTGCAATCTGCGAA-3'] (9). Scrambled aptamer sequence was generated through a random oligonucleotide sequence generator and constrained to have equivalent free energy to the KIT aptamer sequence [5'-TGACGGGAGACTTAAAACGCAAGGGGTGCAGCTATCGCGGAGGCCAAGGGTTCAAGTCGACGGGTAGCTAGGTTGGA-3'] (Oligo Calculator version 3.27, biotools.nubic.northwestern.edu). The aptamer and scrambled sequences were synthesized as an unmodified oligonucleotide, 5'-biotin modification, and 5'-Cy5.5 fluorophore modification (Integrated DNA Technologies, Coralville, Iowa) for various applications.

Cell Culture

We obtained the GIST-T1 line containing a *KIT* exon 11 (heterozygous KIT p.V560_Y578del) mutation (12) from T. Taguchi (Kochi Medical School, Japan) and the GIST882 line containing a *KIT* exon 13 (homozygous KIT K642E) mutation (13) from S. Singer (Memorial Sloan Kettering Cancer Center, New York). Pancreatic cancer cell lines, Panc-1 and MiaPaCa-2 were obtained from ATCC. The mouse ovarian surface epithelial cell line ID8 was provided by D. Schlaepfer (University of California, San Diego), and the human ovarian cancer cell line SK-OV-3 was provided by D. Stupack (University of California, San Diego). All cell lines were cultured as previously reported. GIST-T1, ID8, Panc-1, MiaPaCa-2 and SK-OV-3 were grown in DMEM with 10% FBS, 1% penicillin/streptomycin (Mediatech, Manassas, VA), and 2 mM glutamine (Mediatech) (12,14–16). GIST882 were grown in RPMI with 20% FBS, 1% penicillin/streptomycin (Mediatech), and 2 mM glutamine (Mediatech) (13). The human mast cell line HMC 1.2 (obtained from I. Pass, Sanford Burnham Prebys Medical Discovery Institute, San Diego) was cultured in Iscove's Modified Dulbecco's Medium (IMDM) (Gibco) with 10% FBS, 1% penicillin/streptomycin and 1.2 mM 1-Thioglycerol (Sigma) (17).

ID8 cells, a mouse ovarian cancer cell line, were used to establish a conditional KIT expression cell line using the Sleeping Beauty based transposon system. Briefly, ID8 cells were co-transfected with plasmids containing the *KIT* gene (flanked by the inverted terminal repeats) and a transposase-encoding plasmid (18,19). Stable transgenic cells were selected with hygromycin. KIT expression was controlled by a doxycycline (Dox) inducible

promoter and transgenic cells were detectable by constitutive green fluorescence protein (GFP) expression.

Additionally, a GIST-T1 with constitutive GFP expression was created for use in mouse imaging experiments. Briefly, the GIST-T1 line was transduced by lentivirus with GFP-expressing plasmid. Stable cell lines were created by puromycin selection.

Flow Cytometry

Cells were harvested from monolayer cell cultures using trypsin 0.05% (HyClone) or Accutase (Sigma-Aldrich). Cells were washed in cold Phosphate Buffered Saline (PBS) with 1% FBS. 5'-biotynylated aptamers were incubated with streptavidin-phycoerythrin (SA-PE, Prozyme, Hayward, CA) for 10 minutes in the dark at room temperature. Cells were then treated with fluorophore conjugated aptamer for one hour at room temperature. Cells were then washed with PBS buffer three times and resuspended in PBS for flow cytometry analysis (BD FACSCalibur, San Jose, CA). PE anti-human c-KIT antibody (Clone 104D2, BioLegend, San Diego, CA) was applied in 1:20 dilution for cell staining. FlowJo software was used to analyze the Flow cytometry data.

Ligand Competition Assay

Aptamer specificity was also tested through a competition experiment using the KIT ligand also known as stem cell factor (SCF). GIST-T1 cells were incubated with biotinylated-human-SCF (Arco Biosystems, Newark, DE) conjugated to streptavidin-PE in the presence of unmodified anti-KIT or scrambled aptamer for one hour. Cells were washed thoroughly and resuspended in PBS for analysis by FCM to quantify SCF-bound cells in each condition.

Confocal Immunofluorescence Microscopy

Cells were plated on glass-bottomed well slides and cultured to 50% confluency. Cells were washed thoroughly with PBS and then incubated with pre-conjugated aptamer-SA-PE (400 nM) for one hour at room temperature. Cells were then fixed in 4% paraformaldehyde (Thermo Fisher Scientific), washed and counter-stained with DAPI (1:50,000, Thermo Fisher Scientific).

Fluorescent dextran 10 was used for probing general fluid-phase endocytosis (macropinocytosis and micropinocytosis)(20). We used CF488A Dextran (Biotium, Inc. CA) to study the localization of the anti-KIT aptamer on non-permeabilized live cells. Two hundred thousand GIST-T1 cells were seeded in a 24-multiwell plate (Ibidi USA, Inc.) 24 hours before the treatment. Cells were treated with 10 kDa CF488A Dextran (3nM) and aptamer-PE conjugate (400nM) for 1 hour at 37°C. Cells were thoroughly washed with dPBS with $MgCl_2$ and $CaCl_2$ (Thermo Fisher Scientific) and fixed for 5 minutes with 1% PFA. Fixed cells were then washed again and counter stained with DAPI (1:500) (GeneTex, Inc.). Z-stacks at 63X magnification with LSM880 confocal (Zeiss) were acquired. The images were analyzed with Zen software (Zeiss) to measure the localization of fluorescent signals. For each z stack, the maximum intensity projection was generated followed by fluorescence intensity plots to measure and calculate individual channel intensity.

OCT sections (7 μm) of primary human resected GISTs were obtained under our IRB-approved protocol. Sections were washed thoroughly, labeled with PE-labeled aptamer for one hour at room temperature and permeabilized with 70% ethanol. OCT sections were then counter-stained with DAPI. Fluorescence intensity was visualized with A1R confocal microscope (Nikon, Japan).

Cell Lysate Preparation and Western Blotting

Cells were homogenized in RIPA buffer (Thermo Fisher Scientific) containing protease and phosphatase inhibitors (Cat# A32959, Thermo Fisher Scientific). Protein concentrations were determined. The lysates were then loaded and separated by SDS–PAGE before transfer to a nitrocellulose membrane (BioRad, Hercules, CA). Membranes were incubated with primary anti-KIT antibody (1:1,000, Cell Signaling Technology, Danvers, MA). Secondary antibody horseradish peroxidase-conjugated anti-mouse IgG (1:5,000, Invitrogen, Carlsbad, CA) was added and antibody complexes were detected by the ECL system.

Primary Tumor Dissociation and Single Cell Suspension

Fresh tumor tissue was dissociated into single cell suspensions using the gentleMACS Dissociator (Miltenyi Biotec, San Diego, CA) as previously described (21). Solid tissues were cut into 5-mm size pieces and were transferred to a gentleMACS C-Tube containing RPMI media and MACS human tumor dissociation enzyme cocktail (Miltenyi Biotec) according to manufacturer's instructions for tough tumor tissue (h_Tumor_01). The sample was then passed through a 70 μm filter, and tumor cells were collected following centrifugation. Cells were then labeled using the flow cytometry approach described above.

Cell Viability Assay

Single cell suspensions of tumor cells were seeded at 5,000 cells per well on a 96-well plate (Corning, Lowell, MA). The cells were grown for 48 hours and subsequently treated with 5-, 10- or 20-μM of unmodified KIT or scrambled aptamer for 24-, 48- or 72-hour time points. Cell viability was analyzed by CellTiter-Glo Luminescent Assay (Promega, Madison, WI) and luminescence measured on the Tecan Infinite 200 microplate reader (Tecan, Männedorf, Switzerland).

Generation of Tumor Xenograft Models

Tumor xenograft models were created using the GIST-T1 cell line. Five million cells were injected subcutaneously into the right flank of 5- to 6-week-old *nu/nu* mice (The Jackson Laboratory, Bar Harbor, ME) and allowed to grow until tumor volume was 100–200 mm^3. Mice were then euthanized and tumors were harvested for *ex vivo* analysis.

GFP-labelled GIST-T1 cells were also used to create an intraperitoneal xenograft GIST model. Five- to 6-week-old *nu/nu* mice (The Jackson Laboratory) were injected with 5 million cells intraperitoneally. Mice were monitored weekly for tumor growth by visual inspection and In Vivo Imaging System (IVIS) imaging as described below.

Ex vivo Detection and Animal Imaging

Ex vivo imaging was performed on resected subcutaneous GIST-T1 xenografts. Tumor pieces were labeled with pre-conjugated aptamer-SA-PE (400 nM) in PBS for one hour and then washed thoroughly. Tumor pieces were then imaged using the IVIS system (PerkinElmer, Waltham, MA). Imaging and quantification were performed with Living Image software (PerkinElmer).

Preparation for *in vivo* imaging was done by feeding with an alfalfa-free diet prior to the date of imaging. Anesthesia was induced with isoflurane (2.5% isoflurane, 3 L/min, 5 minutes). Tumor growth was monitored by placing mice in the supine position and GFP fluorescence signal was detected using the IVIS system. After one month from intraperitoneal injection of cells, mice were anesthetized and injected intraperitoneally with aptamer (either KIT or scrambled). Mice were randomly assigned to treatment groups. The aptamer used for live imaging experiments were either directly conjugated to Cy5.5 or pre-conjugated with streptavidin-Cy5.5 (Rockland Immunochemicals, Limerick, PA) with a biotinylated aptamer. Two hours after injection, mice were euthanized, a laparotomy was performed, and *in situ* imaging was performed. Images were acquired using the GFP and Cy5.5 filters, which were normalized to background signal per manufacturer's protocol.

Statistical Analysis

Statistical analyses were performed using Prism GraphPad 7 (GraphPad Software, La Jolla, CA). The investigators were not blinded to allocation during experiments or outcome assessment. Two-tailed unpaired Student's *t*-tests with Welch's correction or one-way ANOVA for multiple comparisons when appropriate were used to determine statistical significance.

Results

KIT aptamer specifically binds GIST cells

We first tested the specificity of the anti-KIT aptamer to bind cells in a KIT-dependent manner. A stable transgenic ID8 cell line was established using a transposon-based plasmid for the integration of c-*KIT* (human) gene into the mouse cell genome. The cell line had c-*KIT* gene expression under a doxycycline (Dox) inducible promoter, as verified by western blot (Fig. 1A). Next, KIT protein expression on the cell membrane was assayed by staining non-permeabilized cells with fluorophore-conjugated anti-KIT aptamer followed by flow cytometry (FCM). An anti-KIT monoclonal antibody was used as a positive control to compare the binding of the anti-KIT aptamer. FCM analysis demonstrated that both the anti-KIT aptamer (32.8% vs 0.05%) and antibody (29.3% vs. 0.04%) bound KIT expressing cells only in the presence or absence of doxycycline (+Dox), respectively, indicating that binding of the aptamer is comparable to the monoclonal anti-KIT antibody (Fig. 1B).

We next confirmed high KIT protein expression in two GIST cell lines [GIST-T1 (KIT V560-Y579Δ5) and GIST882 (KIT K642E)] by western blot (Fig. 1C). Two pancreatic cancer cell lines, Panc1 and MiaPaca2 were utilized as negative controls and had undetectable KIT expression (Fig. 1C). The control scrambled and KIT aptamers were tested

in a dose titration experiment by labeling 1 million GIST-T1 cells to determine the optimal concentration for aptamer-target binding. The aptamer demonstrated binding in a dose-dependent manner while the control scrambled sequence had little binding at any dose, further demonstrating the specificity of the anti-KIT aptamer against the KIT protein expressed on the cell surface (Fig. 1D). The aptamer binding was saturated at 400 nM, and this concentration was used for all subsequent experiments.

Next, FCM analysis was performed on the two *KIT*-mutant GIST cell lines. The geometric mean of the histogram plots from each treatment was divided by the geometric mean of the corresponding unstained cells to obtain the Normalized Geometric mean value. Two independent experiments were performed for each condition. We observed that the anti-KIT aptamer fluorescence intensity was significantly higher than scrambled control aptamer for GIST-T1 (Normalized Geometric Mean [GM] 48 vs. 3.1) and GIST882 (Normalized GM 52.6 vs. 4.2). In contrast, the pancreatic cancer cell lines had KIT aptamer binding that was low magnitude and was comparable to the scrambled aptamer with Panc1 (Normalized GM 3.1 vs. 2.5) and MiaPaCa2 (Normalized GM 2.9 vs. 1.9, respectively). In both positive and negative cell lines, KIT antibody had comparable binding patterns to the KIT aptamer: (GIST-T1 Normalized GM 48.0 vs. 65.2; GIST882 Normalized GM 52.6 vs. 45.4; Panc1 Normalized GM 3.1 vs. 1.2; MiaPaCa2 GM 2.8 vs. 1) (Fig. 1E–F). Additionally, the anti-KIT aptamer reduced binding of PE-labeled KIT ligand (SCF) compared to a negative control (Normalized GM 9.5 vs.57.9, respectively), indicating that aptamer binding resulted in inhibition of SCF binding to KIT. The control scrambled aptamer was not associated with similar inhibition of SCF binding (Normalized GM 57.9 vs. 59.5, respectively) (Fig. 1G–H). Taken together, these experiments demonstrate that this anti-KIT aptamer binds the KIT receptor in a specific manner.

KIT aptamer binds to other cancer cells expressing KIT

We also tested a *KIT* mutant mast cell line, HMC 1.2 (*KIT* G560V and D816V) (22,23), and a human ovarian cancer cell line SK-OV-3 (*KIT* Wild-type) (cBioPortal for Cancer Genomics) for anti-KIT aptamer binding. Higher expression of KIT receptor protein was detected by western blot in the HMC 1.2 as compared to the SK-OV-3 cell line (Supplementary Fig. 1A). This difference was also detected in the flow cytometry data with higher KIT aptamer binding to the HMC 1.2 cells (Normalized GM 94.2) as compared to the SK-OV-3 cells (Normalized GM 28.3). The scrambled aptamer had lower background binding in both the HMC 1.2 and SK-OV-3 cells (Normalized GM 1.9 and 6.8, respectively) (Supplementary Fig.1B–C). Taken together, the data demonstrates that the KIT aptamer can be a useful reagent for KIT detection in other cancers that overexpress this receptor.

KIT aptamer cellular localization

We next examined cellular localization of the anti-KIT aptamer in GIST-T1 and GIST882 cells by immunocytochemistry. Both cell lines demonstrated a similar pattern of anti-KIT aptamer localization at punctate foci consistent with either plasma membrane or intracellular aggregates (Fig. 2A–B). By contrast, the scrambled aptamer demonstrated significantly less fluorescence and was generally distributed in a diffuse pattern that may be due to non-specific cell binding.

Cellular localization of the anti-KIT aptamer was further probed by co-staining with fluorescent dextrans, which are readily internalized through fluid-phase endocytosis. Confocal immunofluorescence demonstrated that the anti-KIT aptamer colocalizes with the CF488A Dextran. Additionally, the analysis of the fluorescence intensity profiles of the signal for the aptamer and the dextran indicated colocalization of the anti-KIT aptamer with cellular vesicles. The scrambled aptamer did not colocalize with any structure in the cells. This data strongly suggests that the aptamer is internalized in GIST cells following KIT receptor binding and is retained within intracellular vesicles. (Fig. 2C–E).

KIT aptamer colocalizes with KIT antibody

Next, we examined the binding and localization of the KIT aptamer as compared to KIT antibody. Cells were co-incubated with both the anti-KIT antibody and anti-KIT DNA aptamer. Cells were then analyzed by FCM (Fig. 3A–B). The fluorescence intensity of the KIT aptamer binding was diminished in the presence of KIT antibody (GIST-T1: GM 246.0 vs. 123.0; GIST882: GM 146.0 vs. 62.0, respectively). This observation suggests that there is either competitive or allosteric targeting of the KIT receptor. This was evident in both the GIST-T1 and GIST882 cell lines. This observation was further corroborated by immunocytochemical analysis. Co-incubation of the anti-KIT aptamer and antibody with live cells resulted in co-localization of signals suggesting that both molecules bound similar aggregates of KIT receptors (Fig. 3C).

KIT aptamer has minimal effect on cell viability

Treatment with anti-KIT aptamer inhibits SCF binding to GIST cells (Fig. 1G–H). In turn, this may inhibit KIT receptor-mediated cell signaling pathways and cell viability. We tested this in GIST-T1 and GIST882 cells by assessing cell viability following treatment with unmodified scrambled or KIT aptamer. Cells were treated at different concentrations (5, 10, and 20 μM), and analyzed for cell viability at 24-, 48- and 72-hour time points. GIST-T1 cells had a decrease in cell viability after treatment with the aptamer compared to the scrambled control (5uM at 24hrs: 90.7% [SD, 2.0], 48hrs: 87.6% [SD, 0.7], 72hrs: 73.9% [SD, 5.9], $P<0.001$). Although there as an observed time-dependent effect, the change in cell viability did not differ between the 5, 10, and 20 μM doses (Fig. 4A). In the GIST882 cell line, there was no significant change in cell viability over time (5uM at 24hrs: 94.2% [SD, 8.9], 48hrs: 101.8% [SD, 2.1], 72hrs: 98.5% [SD, 3.6], $P=0.88$) (Fig. 4B) Similar values were observed for all doses tested. Although there was a difference between the sensitivity of the GIST-T1 and GIST882 cell line, the anti-KIT aptamer generally had minimal or no intrinsic cytotoxic effect on GIST cells. Additionally, the aptamer concentrations tested here were several log-fold higher than the concentration used for cell binding experiments (400 nM). This strongly suggests that the aptamer has negligible adverse cytotoxic effect when utilized for *in vitro* or *in vivo* applications (24).

KIT aptamer binds primary human GIST cells

Next, we tested the capability of the anti-KIT aptamer to bind primary human GIST cells. We utilized several tumor samples encompassing a range of primary tumor locations and mutational profiles (Fig. 5A). KIT aptamer bound cells with several log-fold higher affinity than the scrambled control in all samples tested (GIST#1: GM 35.8 vs. 8.1; GIST#2: GM

407.0 vs. 99.0; GIST#3: GM 239.0 vs. 12.4, respectively). Moreover, we compared the aptamer staining to KIT antibody staining. Fluorescence intensity of the aptamer was higher than antibody in GIST #2 (GM 407.0 vs. 173.0), similar in GIST #3 (GM 239.0 vs. 313.0) and lower in GIST#1 (GM 35.8 vs. 114, respectively) (Fig. 5B–C).

Next, we tested the ability of the KIT aptamer to label cells from tissue specimens on glass-mounted slides. Two resected GISTs were labeled with either KIT or scrambled aptamer and visualized by confocal microscopy (Fig. 5D). KIT aptamer binding demonstrated diffuse binding with some perinuclear enhancement. The staining pattern likely differs from prior immunocytochemistry as these samples were permeabilized at the time of labeling. The staining pattern was similar for a GIST with a *KIT* exon 11 mutation (GIST #4) and one with a *PDGFRA* mutation (GIST #5). In both cases, scrambled aptamer signal was faintly detectable. This indicates a potential application of the anti-KIT aptamer as a reagent for the pathological identification of primary patient GISTs by aptamer-based staining.

KIT aptamer binds GIST tumors *ex vivo* and *in vivo*

Lastly, we tested the capacity of the KIT aptamer to bind GIST xenografts either *ex vivo* or *in vivo*. First, we harvested GIST-T1 xenografts grown subcutaneously in *nu/nu* mice. Tumors were fragmented and labeled with either anti-KIT or scrambled aptamer. Retention of aptamer signal was assessed using the IVIS system. Representative images from three xenograft tumors are shown (Fig. 6A). KIT aptamer had a higher proportion of PE-positive tumors (11/13, 84.6%) compared to scrambled aptamer (2/10, 20%). Moreover, the median fluorescence intensity for the scrambled aptamer was significantly lower than for the KIT aptamer [5.6×10^7 versus 7.5×10^7 counts; P=0.01] (Fig. 6B).

Next, we examined KIT aptamer binding in an intraperitoneal (IP) model of GIST. GIST-T1-GFP cells were used for this model in order to visualize IP tumor burden. One month after IP injection, mice underwent IP injection of either KIT-Cy5.5 or scrambled-Cy5.5 aptamer. Binding was assessed after 2 hours by IVIS (Fig. 6C). Accuracy of tumor binding was assessed by the ratio of Cy5.5 signal to GFP signal for each individual tumor, thus acting as internal controls. Forty percent (4/10) of the scrambled aptamer group had Cy5.5 signal detected above background fluorescence while 85% (11/13) of the KIT aptamer group had Cy5.5 signal detected above background fluorescence (Fig. 6D). Additionally, the median signal intensity of scrambled aptamer overlapping with GIST-T1-GFP signal was significantly lower than that of the KIT aptamer signal [-2.1×10^6 versus 8.6×10^7 counts; P=0.002] (Fig.6E). Collectively, these results suggest that scrambled aptamer binding was non-selective and comparable to background signal, while the KIT aptamer had a high rate of tumor detection and strong signal intensity at the multifocal sites of disease.

Discussion

Gastrointestinal stromal tumor is a disease with well characterized diagnostic markers, including KIT, that also serve as a cognate drug target. Despite widespread use of targeted KIT inhibitors for clinical treatment of GIST, a targeted diagnostic probe is not clinically available. Here, we present the first use of a KIT-specific DNA aptamer for targeted labeling of GIST. We found that the KIT aptamer bound cells in a KIT-dependent manner and is

specific for GIST cells, but not cancer cell lines lacking KIT expression. The KIT aptamer appears to bind the extracellular domain of KIT and is trafficked intracellularly. The aptamer also colocalizes with KIT antibody. Importantly, the KIT aptamer binds primary human GIST cells in a driver mutation-independent manner, suggesting that it has the potential for broad applications. Lastly, the KIT aptamer specifically labels GIST tissue *ex vivo* and *in vivo.* These results represent the first use of an anti-KIT DNA aptamer-based method for targeted detection of GIST.

Although GIST is often associated with KIT mutations, there are a variety of other genes that are implicated in GIST tumorigenesis, including *PDGFRA*, *SDHx* subunits, RAS pathway (*KRAS*, *NF1*, *BRAF*), and gene fusions such as *ETV6-NTRK3* and *FGFR1* fusions (25). However, even non-*KIT* mutant GIST frequently has KIT surface expression. This fact has been leveraged for clinical GIST diagnosis through immunohistochemistry (4). In the current study, we found that this KIT aptamer efficiently labeled GIST cells that harbor *KIT* exon 11, *KIT* exon 13 and *PDGFRA* mutations. Additionally, the aptamer was effective at labeling both live primary human GIST cells and glass-mounted fixed, permeabilized cells. These scenarios underscore the potential applications that a KIT aptamer may be utilized for in GIST diagnosis.

But it is important to consider that as compared to immortalized cell lines, primary human tumors are markedly heterogenous. We found that primary human GISTs had differential labeling with both the KIT aptamer and the KIT antibody control. We found that the aptamer had higher, lower, or equivalent fluorescence intensity as antibody. However, these differences reflect the inherent variations related to tumor heterogeneity and the expected limitations with any single diagnostic approach.

There have been several studies that have tested the capacity of KIT antibody-conjugates to perform a variety of tasks based on KIT-specific targeting. Prior work by our group has demonstrated the feasibility of a near-IR conjugated KIT antibody to be used for intra-abdominal imaging of GISTs (26). Another group developed a radiolabeled KIT antibody for imaging in a mouse model (27). Several groups have utilized KIT antibodies as a targeting system for delivery of chemotherapeutic agents or other cytotoxic approaches (28,29). Others have utilized directly KIT blocking antibodies to abrogate KIT signaling (30,31). During preparation of this manuscript, Shraim *et al.* reported the development and characterization of 2’ fluoro-pyrimidine-modified RNA aptamers against the KIT receptor kinase domains (*KIT* wild type, *KIT* D816V and *KIT* D816H). Interestingly, one of the selected aptamers, V15, specifically inhibited the *in vitro* kinase activity of mutant KIT D816V with an IC_{50} value that was 9-fold lower than sunitinib (32). Here, we present the first usage of a DNA oligonucleotide-based approach for targeted detection of KIT-expressing solid tumors because aptamers have several advantages to antibody-based approaches for cell targeting. First, aptamers are far easier to synthesize than antibodies, which require hybridoma maintenance and complex synthesis protocols. Moreover, aptamers are dynamic molecules that can be readily conjugated to a variety of molecules making them well suited for a variety of clinical applications if the target specificity is high. Lastly, aptamers are small molecules that may have superior tissue distribution and are less likely to promote immunogenicity compared to antibodies. As demonstrated in the primary study by

Zhao *et al.* and reinforced by our findings, this KIT aptamer is an excellent candidate for further development into a clinical diagnostic tool (9).

The FDA approval of pegaptanib (pegylated anti-vascular endothelial growth factor aptamer) marked the introduction of clinical use of aptamer-based therapeutics (33). Imaging and localization studies of the KIT aptamer suggests cellular internalization, which raises the possibility of theranostic applications. For example, conjugation to clinically relevant tyrosine kinase inhibitors (i.e. imatinib, sunitinib or regorafenib) may improve drug delivery permitting dose reduction and increased tolerability of these drugs. Cytotoxicity assays suggest that the KIT aptamer itself has minimally intrinsic cytotoxicity. However, conjugation to a cytotoxic molecule may enable a KIT aptamer-conjugate to serve as a targeted treatment for GIST. Additionally, there are several diagnostic clinical roles for the KIT aptamer. Whole body imaging with a KIT aptamer probe could provide tumor specific diagnosis, as well as monitoring of treatment response. The KIT aptamer also could potentially be adapted for *in vitro* use as a liquid biopsy surveillance tool to detect GIST cells in patients at high risk for disease recurrence.

In conclusion, for the first time we report aptamer labeling of human GIST cells, including primary human tumor cells. KIT aptamer labeling was equivalent or superior to the anti-KIT antibody and bound a similar distribution to KIT molecules *in vitro* and *in vivo*. Taken together, these studies provide proof-of-principle for investigating the utility of anti-KIT aptamers for developing novel GIST diagnostics.

Supplementary Material

Refer to Web version on PubMed Central for supplementary material.

Acknowledgements

We thank Biorepository and Tissue technology shared resource for biospecimen collection. Biorepository and Tissue technology shared resource is supported by CCSG Grant P30CA23100. We thank the Cancer Center Microscopy core for providing microscopes and imaging systems. The Cancer Center Microscopy core is supported by the UCSD Specialized Cancer Center Support Grant (NCI) P30 2P30CA023100-28. The microscope LSM880 is supported by NIH S10OD021831 grant to the La Jolla Institute's imaging core facility. We would also like to thank the UCSD Academic Senate Health Sciences Research Grant awarded to PR and JKS for funding the project.

Financial Support:

We appreciate funding support from the Surgical Society of the Alimentary Tract (SSAT) Mentored Research Award (S.B.) and NIH T32 CA121938 Cancer Therapeutics (CT2) Training Fellowship (S.B.). In addition, we appreciate funding support from Hope for a Cure Foundation (J.K.S.), The Life Raft Group (J.K.S.), Kristen Ann Carr Fund (J.K.S.), Lighting the Path Forward for GIST Cancer Research (J.K.S.), The David Foundation (J.K.S.), NIH K08 CA168999 (J.K.S.), NIH R01 CA226803 (J.K.S.), and FDA R01 FD006334 (J.K.S.). Finally, this work was supported by UC San Diego Health Sciences Research Grant (J.K.S. and P.R.).

J.K.S. has research funding from Novartis Pharmaceuticals, Amgen Pharmaceuticals and Foundation Medicine. J.K.S. also serves or served as Consultant to the following organizations: Grand Rounds (2015–19), Loxo Oncology (2017–18), Deciphera (2019), and Roche (2019).

References

1. Ma GL, Murphy JD, Martinez ME, Sicklick JK. Epidemiology of gastrointestinal stromal tumors in the era of histology codes: results of a population-based study. Cancer Epidemiol Biomarkers Prev 2015;24(1):298–302 doi 10.1158/1055-9965.EPI-14-1002. [PubMed: 25277795]
2. Corless CL, Barnett CM, Heinrich MC. Gastrointestinal stromal tumours: origin and molecular oncology. Nature Reviews Cancer 2011;11(12):865–78 doi 10.1038/nrc3143. [PubMed: 22089421]
3. Barnett CM, Corless CL, Heinrich MC. Gastrointestinal stromal tumors: molecular markers and genetic subtypes. Hematol Oncol Clin North Am 2013;27(5):871–88 doi 10.1016/j.hoc.2013.07.003. [PubMed: 24093165]
4. Martin-Broto J, Martinez-Marin V, Serrano C, Hindi N, Lopez-Guerrero JA, Bisculoa M, et al. Gastrointestinal stromal tumors (GISTs): SEAP-SEOM consensus on pathologic and molecular diagnosis. Clin Transl Oncol 2017;19(5):536–45 doi 10.1007/s12094-016-1581-2. [PubMed: 27943096]
5. Tuerk C, Gold L. Systematic evolution of ligands by exponential enrichment: RNA ligands to bacteriophage T4 DNA polymerase. Science 1990;249(4968):505–10 doi 10.1126/science.2200121. [PubMed: 2200121]
6. Ellington AD, Szostak JW. In vitro selection of RNA molecules that bind specific ligands. Nature 1990;346(6287):818–22 doi 10.1038/346818a0. [PubMed: 1697402]
7. Mi J, Ray P, Liu J, Kuan CT, Xu J, Hsu D, et al. In Vivo Selection Against Human Colorectal Cancer Xenografts Identifies an Aptamer That Targets RNA Helicase Protein DHX9. Mol Ther Nucleic Acids 2016;5:e315 doi 10.1038/mtna.2016.27. [PubMed: 27115840]
8. Ray P, Viles KD, Soule EE, Woodruff RS. Application of aptamers for targeted therapeutics. Arch Immunol Ther Exp (Warsz) 2013;61(4):255–71 doi 10.1007/s00005-013-0227-0. [PubMed: 23563807]
9. Zhao N, Pei SN, Qi J, Zeng Z, Iyer SP, Lin P, et al. Oligonucleotide aptamer-drug conjugates for targeted therapy of acute myeloid leukemia. Biomaterials 2015;67:42–51 doi 10.1016/j.biomaterials.2015.07.025. [PubMed: 26204224]
10. Tanno T, Zhang P, Lazarski CA, Liu Y, Zheng P. An aptamer-based targeted delivery of miR-26a protects mice against chemotherapy toxicity while suppressing tumor growth. Blood Adv 2017;1(15):1107–19 doi 10.1182/bloodadvances.2017004705. [PubMed: 29296753]
11. West RB, Corless CL, Chen X, Rubin BP, Subramanian S, Montgomery K, et al. The novel marker, DOG1, is expressed ubiquitously in gastrointestinal stromal tumors irrespective of KIT or PDGFRA mutation status. Am J Pathol 2004;165(1):107–13 doi 10.1016/S0002-9440(10)63279-8. [PubMed: 15215166]
12. Taguchi T, Sonobe H, Toyonaga S, Yamasaki I, Shuin T, Takano A, et al. Conventional and molecular cytogenetic characterization of a new human cell line, GIST-T1, established from gastrointestinal stromal tumor. Lab Invest 2002;82(5):663–5. [PubMed: 12004007]
13. Tuveson DA, Willis NA, Jacks T, Griffin JD, Singer S, Fletcher CD, et al. STI571 inactivation of the gastrointestinal stromal tumor c-KIT oncoprotein: biological and clinical implications. Oncogene 2001;20(36):5054–8 doi 10.1038/sj.onc.1204704. [PubMed: 11526490]
14. Roby KF, Taylor CC, Sweetwood JP, Cheng Y, Pace JL, Tawfik O, et al. Development of a syngeneic mouse model for events related to ovarian cancer. Carcinogenesis 2000;21(4):585–91 doi 10.1093/carcin/21.4.585. [PubMed: 10753190]
15. Barton CM, Staddon SL, Hughes CM, Hall PA, O'Sullivan C, Kloppel G, et al. Abnormalities of the p53 tumour suppressor gene in human pancreatic cancer. Br J Cancer 1991;64(6):1076–82 doi 10.1038/bjc.1991.467. [PubMed: 1764370]
16. Lieber M, Mazzetta J, Nelson-Rees W, Kaplan M, Todaro G. Establishment of a continuous tumor-cell line (panc-1) from a human carcinoma of the exocrine pancreas. Int J Cancer 1975;15(5):741–7 doi 10.1002/ijc.2910150505. [PubMed: 1140870]
17. Nilsson G, Blom T, Kusche-Gullberg M, Kjellen L, Butterfield JH, Sundstrom C, et al. Phenotypic characterization of the human mast-cell line HMC-1. Scand J Immunol 1994;39(5):489–98 doi 10.1111/j.1365-3083.1994.tb03404.x. [PubMed: 8191224]

18. Kowarz E, Loscher D, Marschalek R. Optimized Sleeping Beauty transposons rapidly generate stable transgenic cell lines. Biotechnol J 2015;10(4):647–53 doi 10.1002/biot.201400821. [PubMed: 25650551]
19. Wang H, Boussouar A, Mazelin L, Tauszig-Delamasure S, Sun Y, Goldschneider D, et al. The Proto-oncogene c-Kit Inhibits Tumor Growth by Behaving as a Dependence Receptor. Mol Cell 2018;72(3):413–25 e5 doi 10.1016/j.molcel.2018.08.040. [PubMed: 30293784]
20. Gomes de Castro MA, Hobartner C, Opazo F. Aptamers provide superior stainings of cellular receptors studied under super-resolution microscopy. PLoS One 2017;12(2):e0173050 doi 10.1371/journal.pone.0173050. [PubMed: 28235049]
21. Banerjee S, Corless CL, Miettinen MM, Noh S, Ustoy R, Davis JL, et al. Loss of the PTCH1 tumor suppressor defines a new subset of plexiform fibromyxoma. J Transl Med 2019;17(1):246 doi 10.1186/s12967-019-1995-z. [PubMed: 31362756]
22. Furitsu T, Tsujimura T, Tono T, Ikeda H, Kitayama H, Koshimizu U, et al. Identification of mutations in the coding sequence of the proto-oncogene c-kit in a human mast cell leukemia cell line causing ligand-independent activation of c-kit product. J Clin Invest 1993;92(4):1736–44 doi 10.1172/JCI116761. [PubMed: 7691885]
23. Sundstrom M, Vliagoftis H, Karlberg P, Butterfield JH, Nilsson K, Metcalfe DD, et al. Functional and phenotypic studies of two variants of a human mast cell line with a distinct set of mutations in the c-kit proto-oncogene. Immunology 2003;108(1):89–97 doi 10.1046/j.1365-2567.2003.01559.x. [PubMed: 12519307]
24. L'Italien L, Orozco O, Abrams T, Cantagallo L, Connor A, Desai J, et al. Mechanistic Insights of an Immunological Adverse Event Induced by an Anti-KIT Antibody Drug Conjugate and Mitigation Strategies. Clinical cancer research : an official journal of the American Association for Cancer Research 2018;24(14):3465–74 doi 10.1158/1078-0432.CCR-17-3786.
25. Alkhuziem M, Burgoyne AM, Fanta PT, Tang CM, Sicklick JK. The Call of "The Wild"-Type GIST: It's Time for Domestication. J Natl Compr Canc Netw 2017;15(5):551–4. [PubMed: 28476734]
26. Metildi CA, Tang CM, Kaushal S, Leonard SY, Magistri P, Tran Cao HS, et al. In vivo fluorescence imaging of gastrointestinal stromal tumors using fluorophore-conjugated anti-KIT antibody. Ann Surg Oncol 2013;20 Suppl 3:S693–700 doi 10.1245/s10434-013-3172-6. [PubMed: 23943029]
27. Sogawa C, Tsuji AB, Sudo H, Sugyo A, Yoshida C, Odaka K, et al. C-kit-targeted imaging of gastrointestinal stromal tumor using radiolabeled anti-c-kit monoclonal antibody in a mouse tumor model. Nucl Med Biol 2010;37(2):179–87 doi 10.1016/j.nucmedbio.2009.10.008. [PubMed: 20152717]
28. Abrams T, Connor A, Fanton C, Cohen SB, Huber T, Miller K, et al. Preclinical Antitumor Activity of a Novel Anti-c-KIT Antibody-Drug Conjugate against Mutant and Wild-type c-KIT-Positive Solid Tumors. Clinical cancer research : an official journal of the American Association for Cancer Research 2018;24(17):4297–308 doi 10.1158/1078-0432.CCR-17-3795. [PubMed: 29764854]
29. Fujimoto S, Muguruma N, Okamoto K, Kurihara T, Sato Y, Miyamoto Y, et al. A Novel Theranostic Combination of Near-infrared Fluorescence Imaging and Laser Irradiation Targeting c-KIT for Gastrointestinal Stromal Tumors. Theranostics 2018;8(9):2313–28 doi 10.7150/thno.22027. [PubMed: 29721082]
30. Reshetnyak AV, Nelson B, Shi X, Boggon TJ, Pavlenco A, Mandel-Bausch EM, et al. Structural basis for KIT receptor tyrosine kinase inhibition by antibodies targeting the D4 membrane-proximal region. Proc Natl Acad Sci U S A 2013;110(44):17832–7 doi 10.1073/pnas.1317118110. [PubMed: 24127596]
31. Edris B, Willingham SB, Weiskopf K, Volkmer AK, Volkmer JP, Muhlenberg T, et al. Anti-KIT monoclonal antibody inhibits imatinib-resistant gastrointestinal stromal tumor growth. Proc Natl Acad Sci U S A 2013;110(9):3501–6 doi 10.1073/pnas.1222893110. [PubMed: 23382202]
32. Shraim AS, Hunaiti A, Awidi A, Alshaer W, Ababneh N, Abu-Irmaileh B, et al. Developing and Characterization of Chemically modified RNA Aptamers for targeting Wild type and Mutated c-KIT Receptor Tyrosine Kinases. J Med Chem 2019 doi 10.1021/acs.jmedchem.9b00868.

33. Gragoudas ES, Adamis AP, Cunningham ET Jr., Feinsod M, Guyer DR, Group VISiONCT. Pegaptanib for neovascular age-related macular degeneration. The New England journal of medicine 2004;351(27):2805–16 doi 10.1056/NEJMoa042760. [PubMed: 15625332]

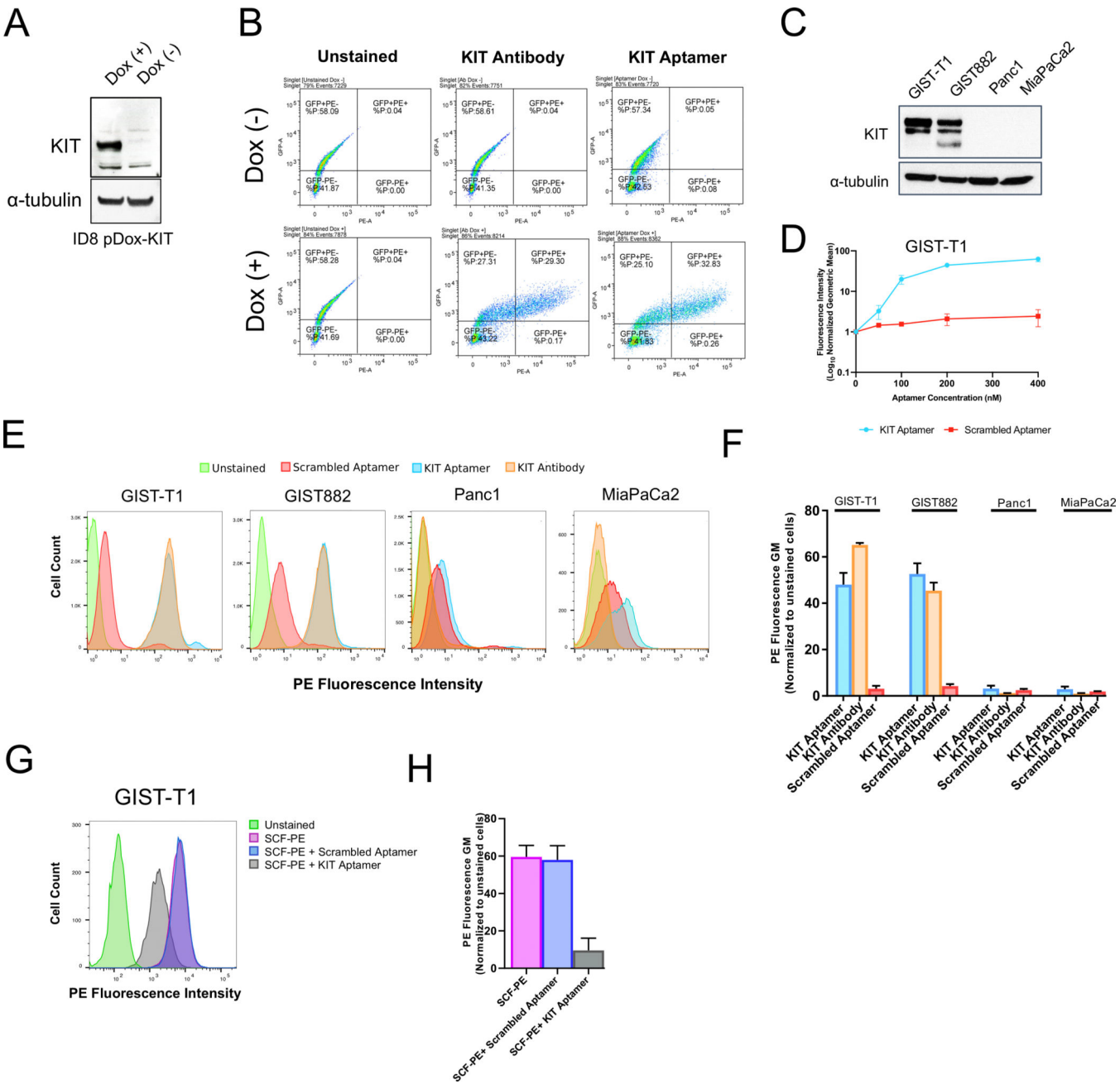

Figure 1: KIT aptamer specifically binds GIST cells.

(A) Western blot of transgenic ID8 cell line with conditional expression of human KIT under doxycycline (DOX) inducible promoter. Alpha-tubulin (α-tubulin) loading control. **(B)** FCM analyses of anti-KIT aptamer and antibody binding to transgenic ID8 cells with conditional KIT expression. Cells were treated with PE-conjugated anti-KIT aptamer, PE-conjugated scrambled aptamer or directly PE-conjugated KIT antibody for one hour at 25C. **(C)** Western blot of KIT protein expression in GIST (GIST-T1, GIST882) and pancreatic cancer (Panc1, MiaPaCa2) cell lines. **(D)** FCM analysis in dose titration of anti-KIT aptamer versus control scrambled aptamer in GIST-T1 cells. **(E-F)** FCM and histogram quantification

(Normalized geometric mean) of anti-KIT aptamer and monoclonal KIT antibody to GIST and pancreatic cancer cell lines. **(G-H)** FCM and histogram quantification (Normalized geometric mean) analysis with co-incubation of anti-KIT aptamer and KIT ligand (stem cell factor, SCF) to GIST-T1 cells. Cells were treated with PE-conjugated SCF and either unlabeled KIT or scrambled aptamer for one hour at 25ºC. The Geometric Mean (GM) of the histogram plots from each treatment were divided by the Geometric Mean of the corresponding unstained cells to obtain normalized Geometric Mean. Data from two independent experiments are plotted with error bars denoting standard deviation of the mean.

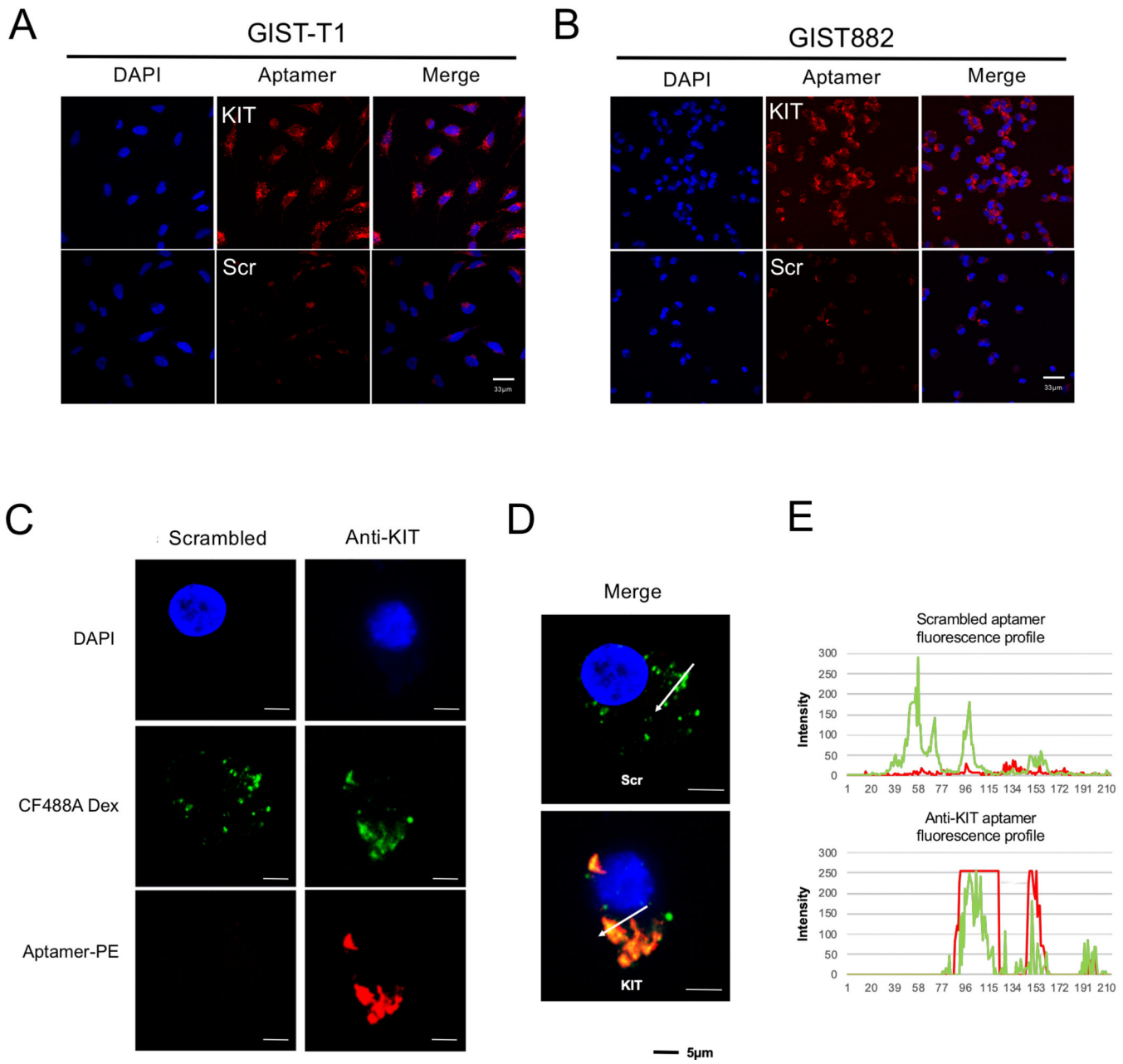

Figure 2: *In vitro* cell imaging of the KIT aptamer in GIST cells.

(A-B) Immunocytochemistry and fluorescence microscopy of live, non-permeabilized GIST-T1 and GIST882 cells with nuclear DAPI (blue), PE-labeled (red) anti-KIT aptamer and PE-labeled scrambled control. Cells fixed with 4% PFA and incubated with PE-conjugated aptamer for one hour at 25ºC. Original magnification is x60 (scale bar, 33 μm). **(C)** GIST-T1 cells were treated with scrambled and anti-KIT aptamers. Single channel images of the scrambled (left) and anti-KIT aptamer (right) shows different aptamer uptake. From top to bottom, DAPI (blue) displaying nuclei, CF488A Dextran (green) highlighting intracellular vesicles, and PE (red) signal localizing the uptake of the aptamers by the cells. **(D)** Merge showing colocalization between green and red indicating that only anti-KIT aptamers were

internalized by the cells. The white arrow indicates the region of the image in which the profile was analyzed. **(E)** Fluorescence intensity profiles of CF488A Dextran and aptamer-PE conjugate showing the colocalization between green and red signal only with anti-KIT aptamer. The control scrambled aptamer did not show any uptake compared to the anti-KIT aptamer (scale bar, 5μm).

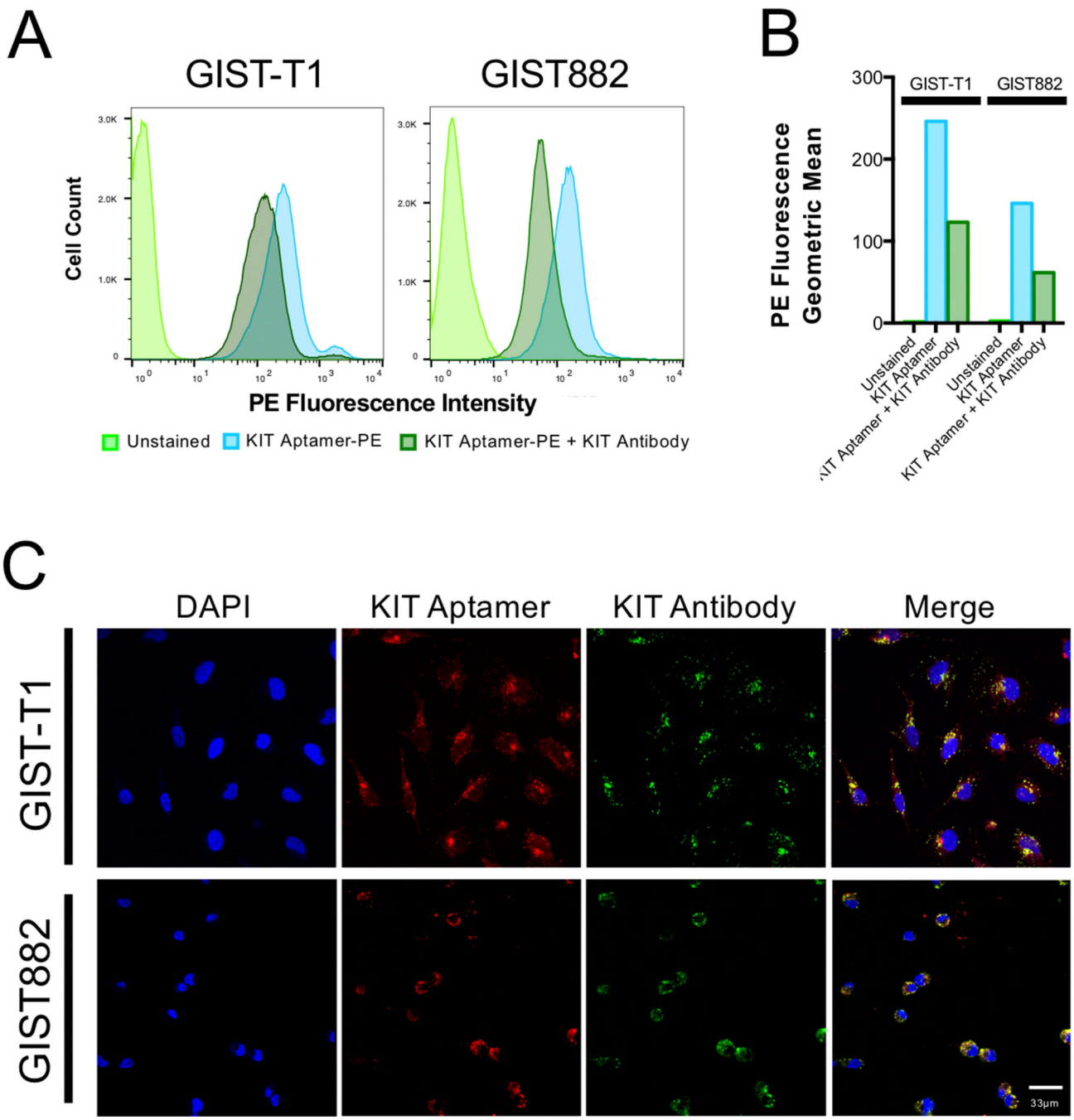

Figure 3: Co-binding of KIT aptamer and KIT antibody in GIST cells.

(A-B) FCM analyses of anti-KIT aptamer and anti-KIT antibody in GIST-T1 and GIST882 cells. Cells were treated with either PE-conjugated anti-KIT aptamer or PE-conjugated anti-KIT aptamer and directly PE-conjugated KIT antibody for one hour at 25ºC. **(C)** Immunocytochemistry and fluorescence microscopy of live, non-permeabilized of GIST-T1 and GIST882 cells with nuclear DAPI (blue), PE-labeled (red) anti-KIT aptamer, scrambled control and directly APC-conjugated KIT antibody (green). Original magnification is x60 (scale bar, 33 μm).

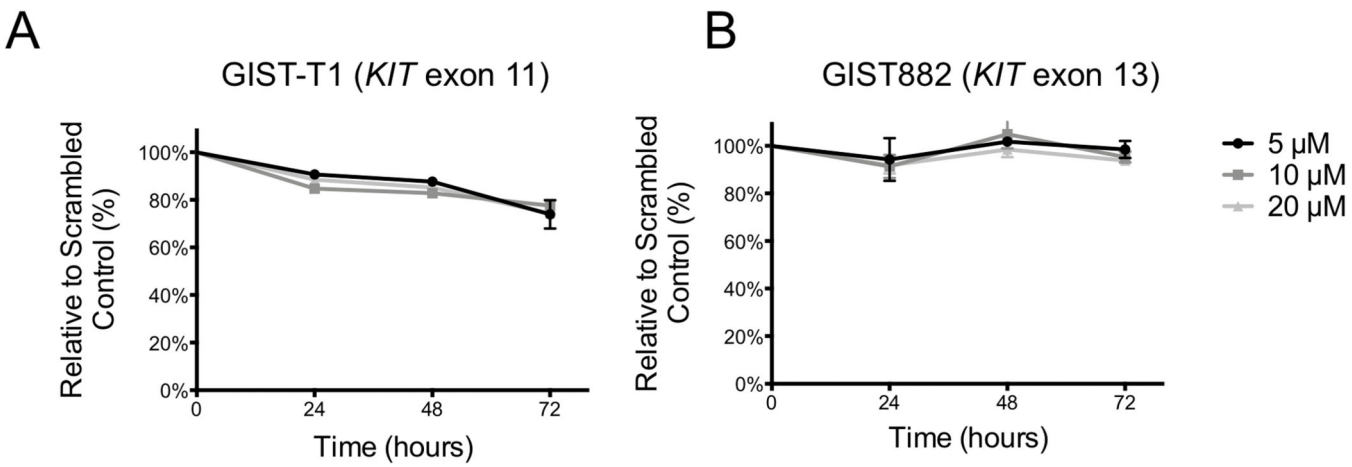

Figure 4: Anti-KIT aptamer has minimal cytotoxicity.

Dose- and time-dependent analysis of cell viability following anti-KIT aptamer treatment of GIST-T1 (heterozygous *KIT* exon 11 mutation) or GIST882 (homozygous *KIT* exon 13 mutation). 5,000 cells were seeded per well and grown for 48 hours then treated with 5-, 10- or 20-μM of unmodified anti-KIT or scrambled aptamer for 24-, 48- or 72-hour time points. Cell viability was analyzed by CellTiter-Glo Luminescent Assay. Mean ± SD (N=3; p-value by linear regression).

A

Tumor Name	Primary Site	Mutation
GIST #1	Gastric	KIT V559I
GIST #2	Gastric	KIT W557_K558>CE
GIST #3	Jejunum	KIT W557_K558del
GIST #4	Duodenum	KIT M552_Y568>N
GIST #5	Gastric	PDGFRA D576_P577ins21

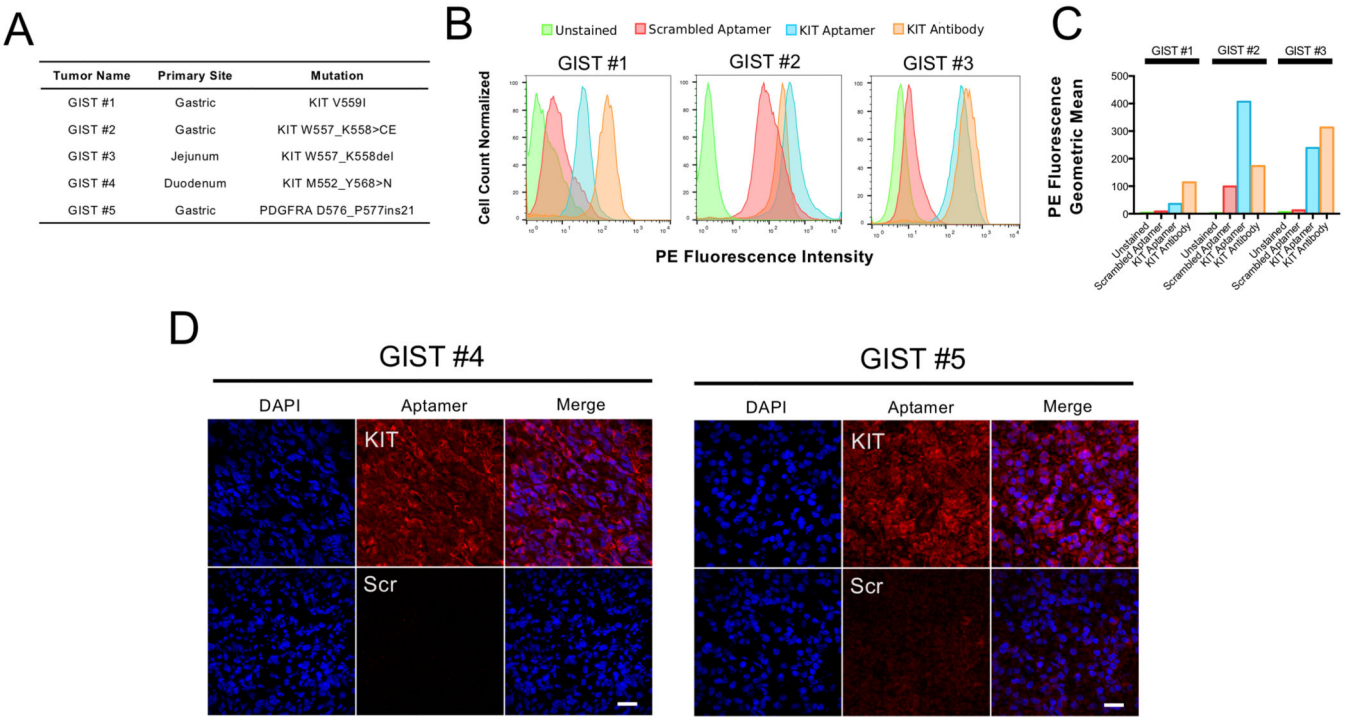

Figure 5: KIT aptamer binds five primary human GIST cells from resected human tumors.

(**A**) Table of five primary GIST tumor sites and driver mutations. **(B-C)** FCM analyses of anti-KIT aptamer and anti-KIT antibody in primary human tumors. Primary tissue was dissociated into single cell suspension and underwent labeling with PE-conjugated anti-KIT aptamer, PE-conjugated scrambled aptamer or directly PE-conjugated KIT antibody for one hour at 25C. **(D)** Immunocytochemistry and fluorescence microscopy of OCT human GIST sections. Slides were stained with nuclear DAPI (blue), PE-labeled (red) anti-KIT aptamer or scrambled control. Original magnification is x60 (scale bar, 50 μm).

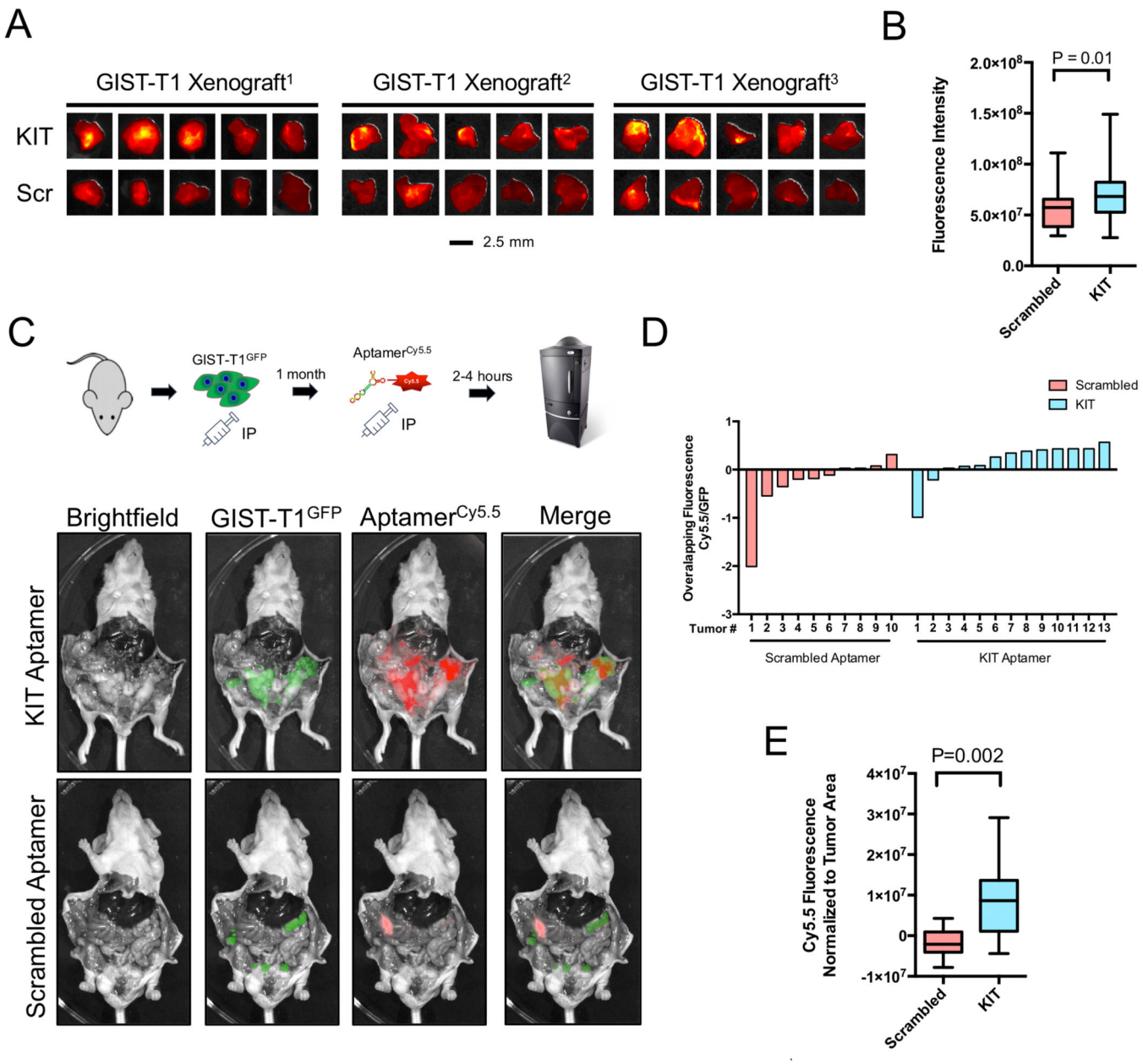

Figure 6: KIT aptamer binds GIST *ex vivo* and *in vivo*.

(A-B) Immunocytochemistry and fluorescence microscopy of *ex vivo* GIST xenograft fragments. Representative images of anti-KIT or scrambled aptamer labeling of xenograft fragments. Fluorescence intensity quantification (Living Image, PerkinElmer) tumor fragments (N=6, p-value by Kruskal-Wallis test). **(C)** Schema demonstrating the experimental workflow of *in vivo* aptamer labeling in an intraperitoneal model of GIST, as well as representative images of GFP-labeled GIST-T1 xenograft *in situ* and Cy5.5-labeled aptamer. **(D)** Waterfall plot analysis of individual tumors with ratio of Cy5.5-labeled aptamer fluorescence intensity to GFP-labeled GIST-T1 xenograft fluorescence intensity (N=10). **(E)** Cy5.5-labeled aptamer fluorescence intensity (Living Image, PerkinElmer)

normalized to tumor area for comparison of *in vivo* labeled IP model of GIST (p-value by Kruskal-Wallis test).